Trafficability Analysis for Lunar/Planetary Exploration Rover using Thrust-Cornering Characteristic Diagram

Genya Ishigami, Keiji Nagatani, and Kazuya Yoshida

***Abstract*— In this paper, a trafficability analysis for the exploration rover is described. A rover traveling on loose terrain often experiences its slippages (wheel slips or vehicle sideslip), and in particular, these slips become larger when the rover traverses on sandy slopes. The authors have investigated traction mechanics of a rigid wheel of the rover on loose terrain with paying attention to slipping behaviors of the wheel. In this paper, based on our previous works regarding the wheel-terrain mechanics, we propose a Thrust-Cornering Characteristic Diagram for trafficability analyses of the rover. The thrust-cornering characteristic diagram consists of various characteristics curves of wheel forces, namely thrust and cornering forces, with various wheel slippage conditions. This diagram provides quantitative criteria for slope traversing capability of the rover on arbitrary angles of slope. The usefulness of the proposed diagram for the trafficability analysis is confirmed through slope traversal experiments using a four-wheel test bed. Further, a steering maneuver control for slope traversing situation is discussed based on the diagram.**

I. INTRODUCTION

The surface mobility using wheeled mobile robots (Rovers) is one of the important technologies for lunar/planetary exploration missions. The rover has to have enough capabilities to travel highly challenging terrains, climb or traverse slopes around craters on the target body. As demonstrated by NASA/JPL Mars Exploration Rovers, a wheel slippage of the rover is one of the particular disturbances when the rover traveled on sandy terrain [1]. A vehicle of a rover also experiences skidding behavior due to the dynamic slips on a contact patch between wheel and loose terrain. In addition, it is easily deduced that the wheel slippage increases when a rover climbs or traverses sandy slopes. Therefore, investigation about the wheel-terrain mechanics is necessary for a better trafficability analysis of the rover, since a dynamic relationship between wheel traction forces and traction load due to the gravity determines the trafficability.

The mechanics of the slipping wheel on loose terrain has been investigated in the field of terramechanics, as in [2]-[4]. For instance, analysis of wheel-soil interaction mechanism and modeling of stress distributions underneath a wheel have been well studied in [2][3]. We have also elaborated a wheel-soil contact model for steering motion analyses of planetary rovers on loose terrain [4].

This work was supported in part by Research Fellowships of the Japan Society for the Promotion of Science for Young Scientists.

Dr. Ishigami is with Massachusetts Institute of Technology, Cambridge, MA 02139 USA (email: ishigami@mit.edu). Profs. Nagatani and Yoshida are with Department of Aerospace Engineering, Tohoku University, Aoba 6-6-01, Sendai, 980-8579 JAPAN (email: {keiji,yoshida}@astro.mech.tohoku.ac.jp).

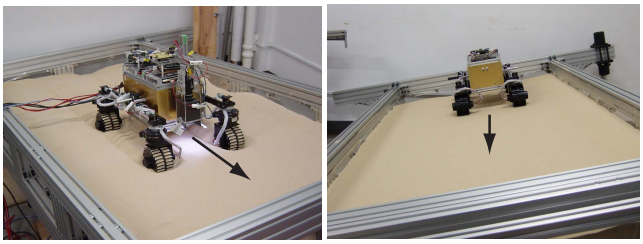

(a) Slope climbing (b) Slope Traversing

Fig. 1. Definition of slope climbing/traversing cases

The slope climbing (Fig. 1-(a)) capability of the rover has been discussed in a plenty of researches [5]-[7]. Seraji proposed a traversability index for rovers on planetary surfaces. This index was expressed by linguistic fuzzy sets that quantify the suitability of the terrain for traversal based on its physical properties, such as slope and roughness [5]. Kuroda et al. conducted slope climbing experiment of a rover by changing gravitational acceleration with considering a similarity model for the rover [6]. However, analytical criteria to determine the slope traversing (Fig. 1-(b)) capability of the rover are still left as an open issue.

In this paper, we propose a diagram for the trafficability analysis of a rover traversing on sandy slopes, based on the wheel model developed in our previous work as in [4], When a rover makes steering maneuvers to traverse on a sandy slope, wheels generate two forces, namely Thrust force and Cornering force. These two forces are characterized by wheel slippages (longitudinal and lateral slips of wheel). Then, we came up with that combining these characteristic curves of forces with correspond to wheel slippages provides an analytical diagram for the trafficability analysis. In this research, this diagram is proposed as *Thrust-Cornering Characteristic Diagram*. Using the diagram, slope traversable or untraversable conditions can be quantitatively determined. The usefulness of the proposed diagram for the trafficability analysis is confirmed through slope traversal experiments using a four-wheel test bed on a tiltable test field covered with loose sand. Further, possible application using the thrust-cornering characteristics diagram to derive appropriate steering maneuvers is presented.

This paper is organized as follows. Section II describes criteria for slop traversing capability. The relationship between thrust/cornering forces and the criteria is presented. In Section III, the analytical model for wheel force is introduced to address the thrust and cornering forces. Then, the Thrust-Cornering Characteristic Diagram is proposed in Section IV along with experimental validation of the proposed diagram.

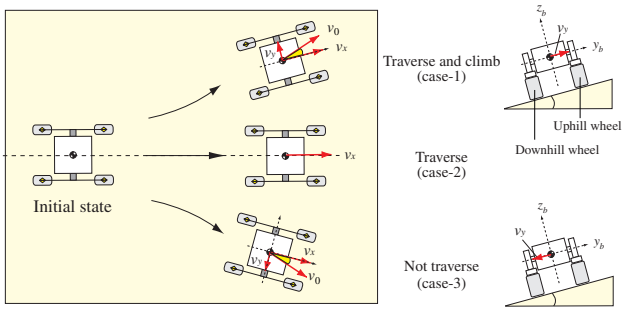

Fig. 2. Slope traversing case: traversable and untraversable

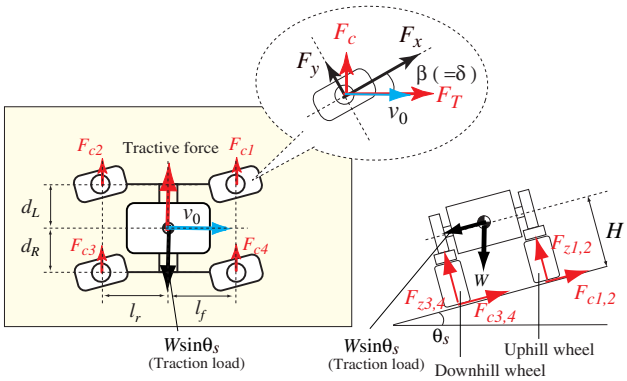

Fig. 3. Force balance on slope traversing case

Section V deals with the possible application using the diagram.

II. SLOPE TRAVERSING CRITERIA

In this section, first, the definition of slope traversing is described. Then, criteria for the slope traversing capability are addressed.

A. Definition of Slope Traversable and Untraversable

When a rover traverses on a side slope as shown in Fig. 2, the motion of the rover can be devided into three ways: 1) traverse and climb (positive lateral velocity of vehicle, $+v_y$), 2) traverse (along with straight line, $v_y = 0$), and 3) not traverse (or slide to downside, negative lateral velocity of vehicle, $-v_y$). This research assumes that cases 1) and 2) are defined as traversable (successful traverse), whereas case 3) is an untraversable. From the figure, it is easily found that the lateral velocity of vehicle must be greater than or equal to zero for successful slope traversal.

B. Criteria for Slope Traversing Capability

An analysis of a slope climbing of a rover is simply determined by a uniaxial force balance between drawbar pull (longitudinal tractive force) of wheel and a vehicle's traction load due to the gravity. However, when the rover traverses a sandy slope, the wheel generates not only longitudinal force but also lateral force since the rover makes steering maneuvers to traverse a slope.

Fig. 3 describes a schematic figure of force balance on slope traversing case. Focusing on the force balance between the tractive force generated by wheels and vehicle traction load, the tractive force must be larger than the traction load in order to achieve its slope traversing. Further, a sideslip of wheel can be observed in slope traversing. This slippage into lateral direction of wheel is measured by slip angle β. The detail of the slip angle is explained in Section III, later. Because of this sideslip, the wheel generates lateral force named Side force F_y. It can be clearly seen that tractive force of vehicle is composed of a summation from F_{c1} to F_{c4}, which are cornering forces of each wheel. Then, the cornering force F_c is given as a function of drawbar pull F_x and side force F_y:

$$F_c = F_x \sin\beta + F_y \cos\beta \tag{1}$$

From the above, the rover can traverse when a summation of cornering forces overcomes the traction load $W \sin\theta_s$. Therefore, one of criteria for the slope traversability is determined as follows:

$$(F_{c1} + F_{c2} + F_{c3} + F_{c4}) \geq W \sin\theta_s \tag{2}$$

On the other hand, another wheel force, F_T, can be composed as seen in Fig. 3. In this research, F_T is named as *Thrust force* consisting of drawbar pull and side force:

$$F_T = F_x \cos\beta - F_y \sin\beta \tag{3}$$

The thrust force needs to be greater than zero so that the rover can travel the slope ahead. Then, another criteria for the traversability is simply defined as:

$$F_{T1} = F_{T2} = F_{T3} = F_{T4} \geq 0 \tag{4}$$

C. Force Equilibrium Point

From the above note, there is an equilibrium point where the traction load is equal to a summation of cornering forces. Then, it is considered that the rover can traverse a slope along with straight line at this force equilibrium point. (This situation is assumed as case-2, shown in Fig. 2.)

The force equilibrium of the vehicle on slope can be written as follows:

$$(F_{c1} + F_{c2} + F_{c3} + F_{c4}) = W \sin\theta_s \tag{5}$$

Here, assuming that the ratio between the required cornering forces for the straight-line traversal, F_{c1} to F_{c4}, is equivalent to the ratio between the vertical forces of each wheel, F_{z1} to F_{z4}, the following equation can be obtained:

$$F_{c1} : F_{c2} : F_{c3} : F_{c4} = F_{z1} : F_{z2} : F_{z3} : F_{z4} \tag{6}$$

note that $(F_{z1} + F_{z2} + F_{z3} + F_{z4}) = W \cos\theta_s$. Then, from (5) and the above equation, the required cornering force for the straight-line traversal can be calculated as follows:

$$\left.\begin{aligned} F_{c1} &= \frac{W \sin\theta_s}{(1+l_f/l_r)\cdot(1+d'_L/d'_R)} \\ F_{c2} &= \frac{W \sin\theta_s}{(1+l_r/l_f)\cdot(1+d'_L/d'_R)} \\ F_{c3} &= \frac{W \sin\theta_s}{(1+l_r/l_f)\cdot(1+d'_R/d'_L)} \\ F_{c4} &= \frac{W \sin\theta_s}{(1+l_f/l_r)\cdot(1+d'_R/d'_L)} \end{aligned}\right\} \tag{7}$$

where, $d'_L = (d_L \cos\theta_s + H \sin\theta_s)$, $d'_R = (d_R \cos\theta_s - H \sin\theta_s)$; l_f and l_r are wheelbase; d_L and d_R are tread; and H is a height of the centroid of the vehicle.

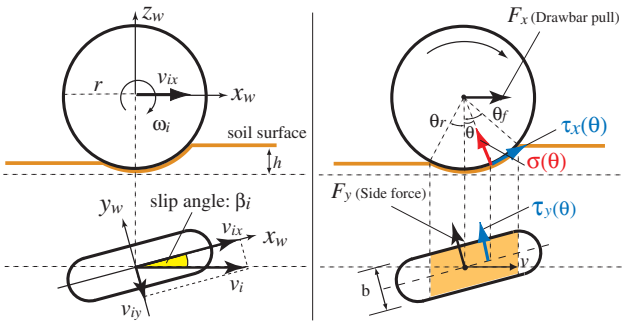

Fig. 4. Analytical model for wheel force

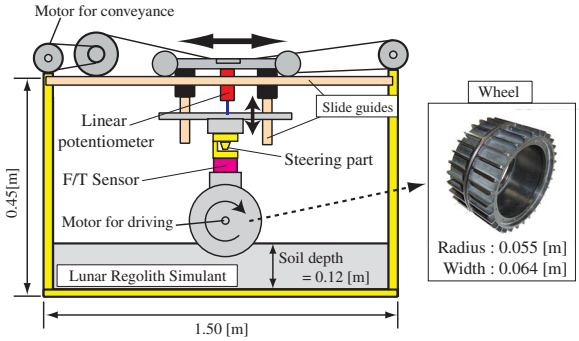

Fig. 5. Schematic view of single wheel test bed

III. WHEEL FORCE CHATACTERISTICS

As indicated in (1) and (3), characteristics of thrust and cornering force of wheel originally depend on drawbar pull F_x and side force F_y. In this section, an analytical model for wheel forces on sandy terrain are introduced based on our previous works as in [4]. First, parameters for wheel slippages into longitudinal and lateral direction are presented. Subsequently, equations to calculate the drawbar pull and side force are described. The analytical model of wheel force is verified using single wheel experiment and characteristics of these forces are addressed.

A. Wheel slips: Slip ratio and Slip angle

It is well known that the wheel slip can be divided into two slips generating around longitudinal/lateral direction of wheel when a rover travels on loose sand.

The slip in the longitudinal direction is expressed by the slip ratio s, which is defined as a function of the longitudinal traveling velocity of the wheel v_x and the circumference velocity of the wheel $r\omega$ (r is the wheel radius and ω represents the angular velocity of the wheel).

$$s = \begin{cases} (r\omega - v_x)/r\omega & (|r\omega| > |v_x| : \text{driving}) \\ (r\omega - v_x)/v_x & (|r\omega| < |v_x| : \text{braking}) \end{cases} \quad (8)$$

The slip ratio assumes a value in the range from -1 to 1.

On the other hand, the slip in the lateral direction is expressed by the slip angle β, which is defined by v_x and the lateral traveling velocity v_y as follows:

$$\beta = \tan^{-1}(v_y/v_x) \quad (9)$$

As described above, slip ratio and slip angle are composed of wheel traveling velocities. Therefore, characteristics of the wheel forces corresponding to these two slip parameters contains wheel velocity metric.

B. Drawbar pull and Side force

A general force model for a rigid wheel on loose soil is presented in Fig. 4. Using the normal stress $\sigma(\theta)$ and the shear stress in x direction $\tau_x(\theta)$, the drawbar pull F_x is calculated by the integral from the entry angle θ_f to the exit angle θ_r [3]:

$$F_x = rb \int_{\theta_r}^{\theta_f} \{\tau_x(\theta)\cos\theta - \sigma(\theta)\sin\theta\} d\theta \quad (10)$$

where, b represents a width of wheel.

The side force F_y acts along the lateral direction of a wheel when the vehicle makes a steering maneuver. We have modeled the side force as follows [4]:

$$F_y = \int_{\theta_r}^{\theta_f} \{rb \cdot \tau_y(\theta) + R_b \cdot (r - h(\theta)\cos\theta)\} d\theta \quad (11)$$

where, R_b is the reaction resistance generated by the bulldozing phenomenon on the side face of the wheel. R_b is given as a function of a wheel sinkage h. $\tau_y(\theta)$ is the shear stress in y direction.

Note that, normal stress σ, and shear stresses, τ_x and τ_y include terrain parameters, such as cohesion, friction angle, and soil deformation moduli. Detailed descriptions for this model is found in [4].

C. Single Wheel Experiment

To validate the analytical model for wheel force, experiments using a single-wheel test bed were conducted. The experimental results were compared with the numerical simulation results obtained from the analytical model, and then, the characteristics of both the drawbar pull and side force were confirmed.

1) Single-wheel test bed: Fig. 5 shows the schematic view of the single wheel test bed. The test bed comprises both a conveyance unit and a wheel-driving unit. The steering angle (which is equivalent to the slip angle in this test bed) is set between the conveyance unit and the wheel. The translational velocity and angular velocity of the wheel are calculated based on the data obtained by the encoders that are mounted on the conveyance motor and wheel-driving motor, respectively. The forces and torques generated by the wheel locomotion are measured using a six-axis force/torque sensor located between the steering part and the wheel. The vessel of the single-wheel test bed is filled with around 10 [cm] (depth) of loose sand, *Toyoura sand*, which is cohesion less loose sand and also well-known as a standard sand for terramechanics research field [8][9]. A wheel with a diameter of 11.0 [cm] and a width of 6.4 [cm] is covered with paddles having heights of 0.5 [cm]. The total load of the wheel is approximately 5.1 [kg].

In the following experiments, the wheel is controlled to rotate with a constant circumference velocity (0.015 [m/s]) by the driving motor mounted inside the wheel. The translational velocity of the wheel is also controlled such that the

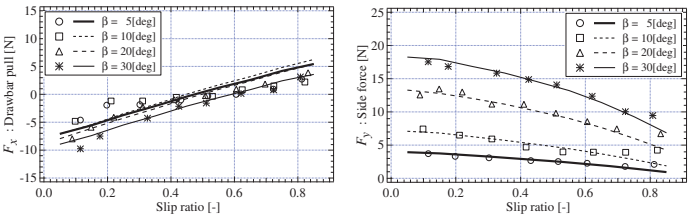

(a) : Drawbar pull (b) : Side force

Fig. 6. Experimental and simulation results

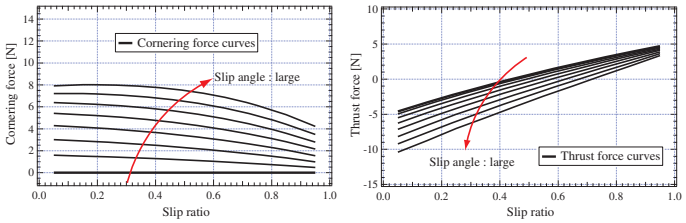

(a) : Cornering force (b) : Thrust force

Fig. 7. Characteristics of cornering and thrust forces

slip ratio of the wheel is set from 0.0 to 0.8 in steps of 0.1. The slip ratio is constant during each run. Further, the value of the slip angle of the wheel is varied from 5° to 30° in steps of 5°.

2) Experimental results: Experimental measurements of a drawbar pull and a side force are respectively plotted in Fig. 6, for each slip angle, 5, 10, 20, and 30 [deg]. Theoretical curves calculated by the analytical model are also shown in the corresponding figures.

The characteristic of wheel forces can be summarized as follows: the drawbar pull increases as the slip ratio increases, but it decreases as the slip angle increases. Also, the side force decreases along with the slip ratio and increases according to the slip angle.

From Fig. 6, it is seen that the differences between the measured forces and the theoretical values are comparatively small. These results validate that the analytical model for wheel force is able to represent the traveling behavior of slipping wheel and the contact forces with a reasonable precision.

IV. THRUST-CORNERING CHARACTERISTIC DIAGRAM AND TRAFFICABILITY ANALYSIS

In this section, the thrust-cornering characteristic diagram is proposed. The trafficability analysis using the proposed diagram is also addressed.

A. Thrust-Cornering Characteristic Diagram

The characteristics of both drawbar pull and side force for various wheel slippages has been clarified in Section III. As defined in (1) and (3), the characteristics of thrust and cornering forces with different slip ratios/slip angles can be elaborated as shown in Fig. 7.

We came up with the following diagram: combining Fig. 7-(a) and (b), the relationship between the thrust force and cornering force can be obtained as a diagram as shown in Fig. 8. This diagram is proposed as Thrust-Cornering Characteristic Diagram in this research.

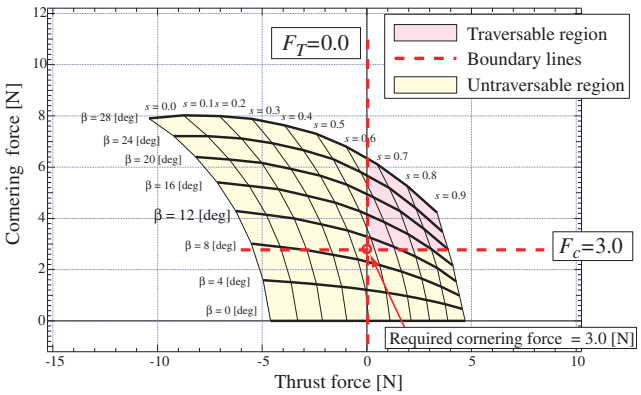

Fig. 8. Thrust-Cornering Characteristic Diagram

The diagram can be applied to any terrain (sandy, muddy, or hard terrains) and any wheel dimensions once terrain parameters and wheel shapes are given to the wheel force model. Also, the diagram contains wheel velocity factors because the diagram consists of the characteristics curves with corresponding to slip ratios/slip angles.

B. Approach of Trafficability Analysis

The trafficability analysis using this diagram is as follows: First, a cornering force of each wheel which balances with a traction load on an arbitrary slope angle can be determined using (7). For instance, a traction load is assumed to be 3.0 [N]. Then, this turns out that the required cornering force to traverse the slope is given as $F_c \geq 3.0$. Also, referring to another criteria for slope traversing capability determined in (4), the required thrust force is given as $F_T \geq 0$. Subsequently, drawing these two boundary lines ($F_c \geq 3.0$ and $F_T \geq 0$) on the diagram, it can be seen that the diagram is divided into two regions, namely traversable/untraversable regions.

Here, as shown in Fig. 3, the steering angle is assumed to be equivalent to the slip angle if the rover successfully traverses the slope in straight ahead. Therefore, the thrust-cornering characteristic diagram determines the trafficability of the rover based on given steering angles: as shown in Fig. 8, it is expected that the rover having more than 12 [deg] of steering angles can traverse and climb the corresponding slope since the characteristics curve of $\beta = 12$ [deg] is larger than the required cornering force and is included in the traversable region.

A computational time for the above analysis takes around 0.5 [sec] (1.66 [GHz] processor). Most of the computational time spends to get whole data which are needed to form the thrust-cornering characteristic diagram.

C. Slope Traversing Experiment and Trafficability Analysis

Slope traversal experiments using a four-wheel test bed were carried out to validate the proposed diagram for the trafficability analysis. In this paper, two cases are addressed; slope traversable and untraversable cases with changing slope angle.

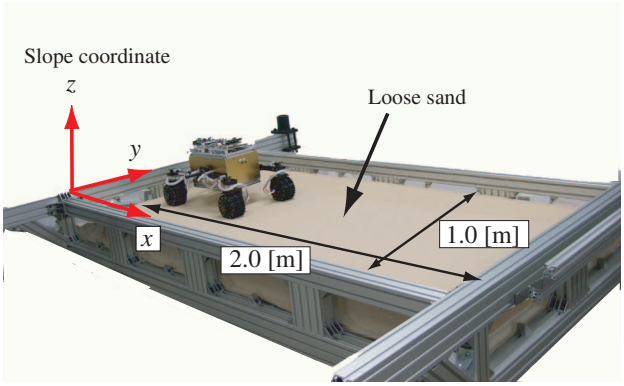

Fig. 9. Overview of the experimental setup

1) Experimental Setup: Fig. 9 shows the overview of the experimental setup with the rover test bed. The test field consists of a rectangular tiltable vessel in the size of 2.0 by 1.0 [m]. The vessel is filled up with 8.0 [cm] depth of Toyoura Sand. The four-wheeled rover test bed has a dimension of 0.44 [m] (wheelbase) $\times$ 0.30 [m] (tread) $\times$ 0.30 [m] (height) and weights about 13.5 [kg] in total. Each wheel of the rover is same as the one used in the single wheel experiment.

In the experiment, each steering angle of all wheels of the rover is controlled to maintain 15 [deg] to the uphill direction of the slope. The experiments are conducted in two cases: in case-A, the slope angle is 5 [deg], and in case-B, it is 10[deg].

2) Trafficability analysis using proposed diagram: The motion traces of the rover in these experiments are illustrated in Fig. 10. From the figures, the rover successfully traversed and climbed in case-A, however, the rover slid down the slope in case-B. It is deduced that the summation of cornering forces must be smaller than the traction load of the rover in case-B.

This difference between traversable/untraversable cases can be explained by using the thrust-cornering characteristic diagram. The thrust-cornering diagrams for uphill/downhill wheels in case-A and case-B are shown in Fig. 11 and Fig. 12. A red circle in each diagram indicates the required cornering force calculated by (7). Also, a blue curve on the diagram denotes the specific thrust-cornering curve when the slip angles of wheels are 15 [deg].

From Fig. 11, it is found that the required cornering forces of both uphill/downhill wheels (red circles) are smaller than the specific thrust-cornering curves (blue curves) when $F_T = 0$. This means that wheels of the rover in case-A generate large enough cornering forces so that the rover can traverse and also climb the slope. However, in case-B as shown in Fig. 12, the specific thrust-cornering curves in either uphill/downhill wheels never exceed the required cornering forces. Also, any curves never overlap into the traversable region at any slip ratios; this means that the rover in case-B cannot traverse the slope in this steering configuration.

The following point must be emphasized: the thrust-cornering characteristic diagram in case-B also indicates that

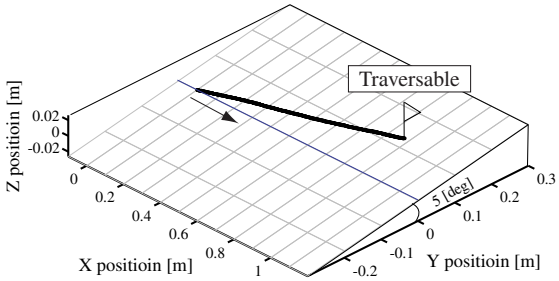

(a): case-A: slope angle 5 [deg]

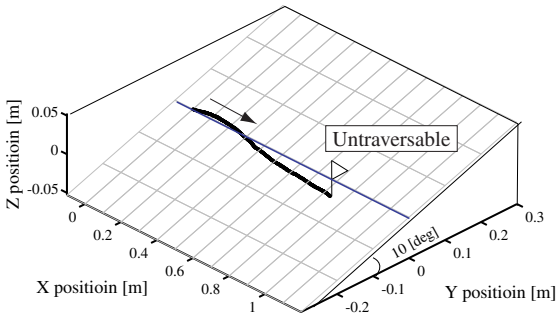

(b): case-B: slope angle 10 [deg]

Fig. 10. Slope traversing experiments

the rover on the slope of 10 [deg] will be able to traverse the slope if the steering angle is appropriately given such that the specific thrust-cornering curve exceeds the required cornering force (i.e. traversable steering angle will be around 20 [deg].)

V. POSSIBLE APPLICATION FOR STEERING MANEUVER CONTROL

In this section, possible application using the thrust-cornering characteristic diagram is concisely addressed.

Through the trafficability analysis described in Section IV, it is found that the thrust-cornering characteristic diagram will be useful to determine appropriate steering angles for successful slope traversing. Also, as discussed in Section II, an equilibrium point where a traction load is equal to a summation of cornering forces is found when a rover traverses a slope with arbitrary steering angles. At this force equilibrium condition, the rover can traverse a slope along with straight line, or without any sideslip of vehicle, and also, a steering angle δ of wheel is equivalent to the wheel slip angle. Therefore, once the required cornering force for slope traversing is given, it is expected that an appropriate steering angle can be found on the thrust-cornering characteristic diagram as an intersection point at which the two boundary lines cross.

Based on this approach, a typical case study is addressed in this paper. Using the trust-cornering characteristic diagrams for case-B (Fig. 12), the steering angles, which correspond to the intersection point of two boundary lines, are determined as 18.9 [deg] for uphill wheels and 19.5 [deg] for downhill wheels. Then, the slope traversing experiment with the derived steering angle to each wheel were conducted and the result is shown in Fig. 13.

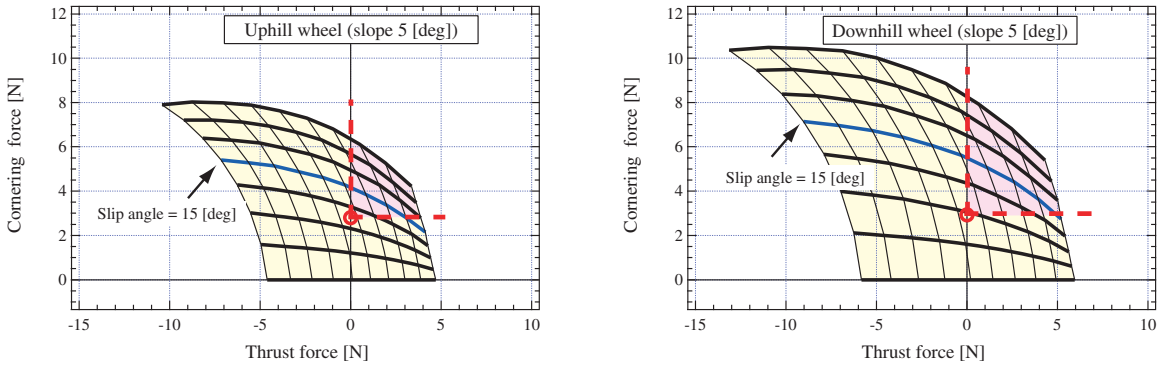

Fig. 11. Thrust-cornering characteristic diagram : case-A (slope angle is 5 [deg])

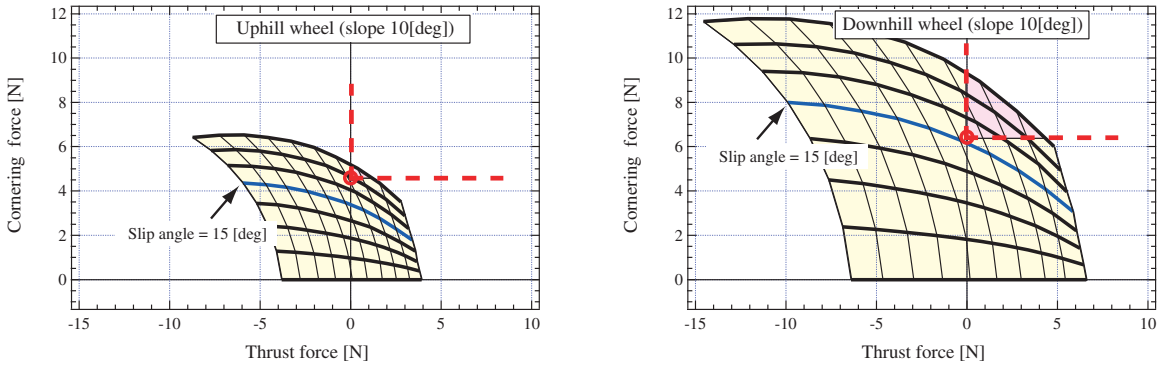

Fig. 12. Thrust-cornering characteristic diagram : case-B (slope angle is 10 [deg])

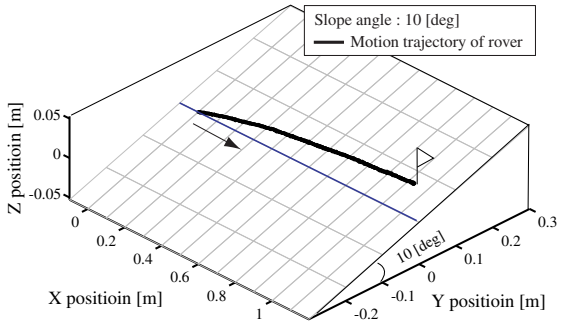

Fig. 13. Slope traversing with steering maneuver using proposed diagram

From the figure, it is clearly seen that the rover can successfully traverse the slope. The error to the straight line indicated as a blue solid line in the figure is less than 7 [cm]. This error is due to an error in the wheel force model including terrain parameter error. However, the result shows that the proposed diagram is useful for a model-based feedforward control to traverse a sandy slope.

VI. CONCLUSION

In this paper, the trust-cornering characteristic diagram has been proposed for the trafficability analysis of the rover. This diagram provides quantitative criteria for slope trafficability of the rover. The usefulness of the proposed diagram has been confirmed through slope traversal experiments using the four-wheel test bed on the tiltable test field. As concisely described in Section V, the proposed diagram can be extended to practical applications, such as calculating appropriate steering angles to traverse a slope.

The trust-cornering characteristic diagram will be useful in performing path planning computation of a vehicle under slipping/skidding conditions. For example, a planetary terrain surface covered with various types of soil can be classified according to traversable/untraversable areas, based on several thrust-cornering characteristic diagrams calculated with various terrain parameters.

REFERENCES

[1] http://marsrovers.jpl.nasa.gov/home/index.html (as of February 2008)

[2] M. G. Bekker; *Introduction to Terrain-Vehicle Systems*, The University of Michigan Press, 1969.

[3] J. Y. Wong; *Theory of Ground Vehicles*, John Wiley & Sons, 1978.

[4] G. Ishigami, A. Miwa, K. Nagatani, and K. Yoshida; "Terramechanics-Based Model for Steering Maneuver of Planetary Exploration Rovers on Loose Soil," *The Journal of Field Robotics,*, Vol. 24, No. 3, pp. 233-250, 2007.

[5] H. Seraji; "Traversability Index: A New Concept for Planetary Rovers," *Proc. of the 1999 IEEE Int. Conf. on Robotics And Automation,* pp. 2006-2013, 1999.

[6] Y. Kuroda, T. Teshima, Y. Sato, and T. Kubota; "Mobility Performance of Planetary Rover in Difference of Gravitational Acceleration," *Proc. of the 2005 IEEE/RSJ Int. Conf. on Intelligent Robots and Systems,* pp. 1413-1418, 2005.

[7] K. Yoshida, N. Mizuno, G. Ishigami, A. Miwa; "Terramechanics-Based Analysis for Slope Climbing Capability of a Lunar/Planetary Rover," *Proc. of the 24th Int. Symp. on Space Technology and Science,* 2004-k-06, 2004.

[8] http://www.toyourakeiseki.com/product-e.htm (as of July 2008)

[9] T. Kobayashi et al; "Load-settlement Characteristics of Japanese Lunar Soil Simulant in Partial Gravity," *Preprints of Space Resources Roundtable VIII,* 2006.